The Budget Study of Cloud/Radition Effects During the TAMEX IOP-2

WEN-SHUNG KAU[1] and SHR-JI WU[1]

ABSTRACT

The lifetime of Mei–Yu fronts over southern China ranges from 3 to 22 days (Chen, 1983), with a nearly continuous cloud band accompanying the front. It is the goal of this study to estimate the cloud and radiative effects on the Mei–Yu front during the TAMEX IOP–2 periods.

The present radiative transfer model is based on a broadband method and involves the transfer of IR and solar radiation for both clear and cloudy regions. To perform radiative transfer calculations and to compare this with observed cloudiness, a diagnostic cloud scheme is adopted in this paper. This cloud scheme is similiar to Geleyn's (1981) approach. After we obtained the model–predicted cloud covers, we then divided into low, middle and high clouds, which overlapped each other to a maximum or minimum degree.

Predicted cloudiness during the TAMEX IOP–2 periods, with the use of ECMWF/ WMO analysis data sets, has shown a reasonable degree of success. The nearly continuous cloud band over the Mei–Yu front is well simulated. This cloud band is dominated by middle–level cloud with several high–level deep cumulus clouds embedded in it. However, the cloudness in general is underestimated by the model, especially for high–level cloud.

Observing the model–predicted cloud cover and OLR fields, we find that the OLR patterns are basically related to the predicted cloud cover. In the Mei–Yu frontal zone the computed OLR value is less than 220 Wm^{-2} and it also has several minimum centers within it. Comparing the predicted OLR patterns with the satellite derived OLR data, we find that simulated patterns are in agreement with the observations. Nevertheless, the OLR fluxes over the Mei–Yu frontal zone and the tropical convection areas, are slightly larger than the observations.

The distributions of the computed radiative heating and cooling rate have very different vertical profiles. For the net radiative heating rates, it is seen that maximum heating for the three computed periods is less than 3.5°C/day and is all located below the high–level cloud base. Neverthless, the biggest net cooling along the Mei–Yu front is much greater than the heating (> 6°C/day) rate and is all concentrated in the upper troposphere. It is also noted that cooling over the Taiwan area is greater than 6°C/day for both the 1200 UTC 16 and 0000 UTC 17 periods.

---

[1] Department of Atmospheric Sciences, National Taiwan University, Taipei, Taiwan, R.O.C.

1. INTRODUCTION

During the transition period from the winter northeast monsoon to the summer southwest monsoon Mei–Yu is a distinctive climatological phenomenon over Taiwan. Within this period, rainfall may be continuous or intermittent for several days up to a few weeks. Synoptically this rainfall is associated with the repeated occurrence of fronts, extending eastward from southern China to the Japanese islands. The front, representing a maximum moisture gradient zone near the surface, is called the Mei–Yu front. From satellite pictures we see a nearly continuous cloud band accompanying the Mei–Yu front. The cloud distribution is not uniform along the Mei–Yu front. Dense clouds may be organized into cloud clusters extending a few hundred kilometers. These cloud clusters (medium–scale cloud clusters) are associated with subsynoptic–scale frontal depressions. In general, meso–scale (meso–β–scale) cloud clusters are embedded in these medium–scale cloud clusters (Ninomiya & Murakami, 1991) . Significant differences in circulation systems and clouds exist between the early and late Mei–Yu season. As shown by Kato (1985) , the Mei–Yu frontal zonal consists mainly of deep cumulus clouds for the period of 10–19 June 1979. On the other hand, two types of clouds are found in the period of 1–20 May 1979, i.e. the active convective cloud exists only at the southern edge of the Mei–Yu frontal zone and the stratiform cloud which covers a wide area of it.

It is well estabilished that clouds are a critical factor in regulating the radiative energy balance of weather systems. Analyses of satellite observed radiances have shown that the radiation budgets at the top of the atmosphere are largely controlled by the cloud field. In general, clouds exert two competing effects on the radiation field of the earth–atmosphere system. On one hand, clouds reflect a significant portion of the incoming solar flux, and on the other, clouds also trap the outgoing thermal infrared flux emitted from the surface and the atmosphere below them. Certain clouds, such as stratus, are primarily responsible for the reflection of solar radiation, whereas others (cirrus) are important greenhouse modulators. The competition of the solar albedo and infrared greenhouse effects determine whether the surface would undergo cooling or warming. Through condensation and precipitation, clouds also have a direct impact on dynamic and hydrological processes in the atmosphere. In an attempt to understand the intricate interactions of radiation, clouds and dynamic processes, Liou & Zhang (1984) performed numerical experiments using a GCM designed for short and medium range weather prediction. There are numerous findings regarding the quantitative effects of cloud/radiation interactions on temperature and cloud prediction in a 10–day prediction experiment. In particular, it has been demonstrated that radiative heating profiles in tropical regions are critical to maintenance of the Hadly circulation.

All the Mei–Yu fronts influencing Taiwan were formed in an area $20°–30°N$ and $100°–130°E$ with a lifetime from 3 to 22 days (an average of 8 days)(Chen, 1983). Therefore, cloud/radiation processes must have significant effects on the Mei–Yu front. The objective of this paper is to estimate the role of clouds and coupled radiative effects on the Mei–Yu front. We chose the TAMEX IOP–2 period as a starting point. In section 2, we briefly described the cloud/radiation parameterization scheme. Results from the cloud/radiation parameterization scheme using ECMWF/WMO analysis data sets from May 16–17 , 1987 are presented in section 3. Finally, conclusions are given in section 4.

2. PARAMETERIZATION OF CLOUD AND RADIATION

2.1 Cloud Scheme

Clouds are a product of complicated interactions between moist convective turbulence with large scale circulations, radiation and microphysical processes. However, most clouds are subgrid–scale, both horizontally and vertically; there is neither a theory nor an observational database which can be used to relate cloudiness to the large–scale variables (Slingo, 1987). Two types of cloud parameterizations are being used in general circulation models. The first is a statistical or diagnostic approach, in which cloudiness is predicted empirically from model variables. The function are chosen to represent the probability of cloud occurring under certain atmospheric conditions. The basic premise of such schemes is that condensation on the smaller scale is part of a larger scale condensation regime related to the synoptic scale situation. These diagnostic schemes have been successful in simulating gross features of observed clouds. The second method uses a prognostic approach, in which the explicit calaulation of cloud water content, involving the formation and evaporation of cloud and rain drops, is made (Sundqvist, 1978). Diagnostic schemes derive cloud cover and occasionally cloud water content from model variables such as relative humidity, vertical velocity, atmospheric stability, cumulus mass flux, wind shear, surface flux etc. The main advantages are the simple treatment and low computational requirments. However, a sound physical basis is lackinng and, in particular, is not capable of dealing with the interaction between optical cloud properties and the hydrological cycle of the numerical model. In prognostic cloud schemes cloud evolution is linked, interactively, to the rest of the model physics (dynamics, radiative transfer, hydrology, convection, turbulence). The development of such a scheme requires the consideration of the advective transport of cloud variables, sub–grid scale transport, cloud microphysics and optical cloud properties. Such a scheme is computationally more expensive than a diagnostic method, although there exist clear advantages.

We will use the diagnostic method to estimate cloudiness in this study. Almost all diagnostic schemes have the same parameterized from as (Geleyn, 1981 ; Slingo & Ritter, 1984, etc.):

$$\eta = [\frac{h - h_c}{1 - h_c}]^2, \quad h > h_c$$
$$0 \quad , \quad h \leq h_c \tag{1}$$

but they differ in the prescription of the threshold value of relative humidity h_c.

With the introduction of the relative humidity threshold, partial cloudiness in the grid box is allowed when large–scale relative humidity(h) is less than 100%. When clouds from it is assumed that they fill the entire layer. The cloudy area and clear region in a grid box are denoted by η and ($1-\eta$), respectively.

In our present program, we used Geleyn's specification of h_c, i.e.,

$$h_c = 1 - \alpha\sigma(1 - \sigma)[1 + \beta(\sigma - 1/2)] \tag{2}$$

where $\alpha = 2$, $\beta = \sqrt{3}$, $\sigma = p/p_x$ and p_x is the surface pressure.

From eq.(2) we could find the maximum value of the h_c is 1. and is located at both σ = 0 and σ = 1, while the minimum of h_c is 0.45 and is around σ = 0.6. These suggest that the cloud is hard to form at both the model's top and bottom layers; however, at the middle of the present model, the cloudiness is very easy to present.

Specification of the overlap that occurs between cloud layers is required for the calculation of radiative transfer in a radiation model, since only the cloud fraction for each model layer is determined by the cloud model. Based on surface observation, there are generally fewer than three cloud decks along the vertical. Accordingly, it appears appropriate to strap the model–generated multilayer cloudiness into at most three cloud decks. For the present model, low, middle, and high clouds fill, respectively, layers (6, 7, 8), layers (4, 5), and layers (2, 3), as indicated in Figure 1. The top four layers and the bottom layer are specified as being cloudless.
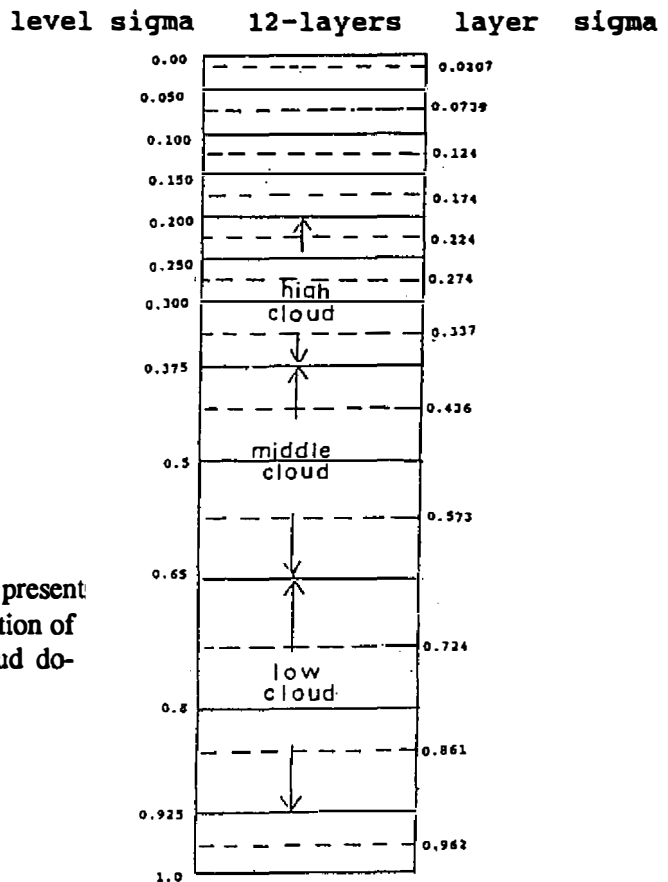

Fig. 1. Vertical grid structure in the present model, along with specification of high, middle, and low cloud domains.

The total cloud cover for each horizontal grid space is determined by two steps. The first step involves calculation of the cloud cover for each deck. Then, the total cloud cover may be evaluated by using certain overlap assumptions. In our present model, we have used the maximum scheme in determining the cloud deck cover.

To determine the total cloud cover, we must consider the effect of overlap between cloud decks. Several assumptions can be made in the overlap configurations. There are :

1) Maximum overlap: In this case, the total cloud is given by

$$\eta = max(\eta_l, \eta_m, \eta_h) \qquad (3)$$

2) Random overlap: This configuration assumes that clouds overlap each other in a statistically random manner. Thus, the total cloud cover may be expressed by

$$\eta = 1 - (1 - \eta_l, 1 - \eta_m, 1 - \eta_h) \qquad (4)$$

3) Minimum overlap: This configuration assumes that clouds overlap each other in a minimum fashion.

$$\eta = min(1, \eta_l + \eta_m + \eta_h) \qquad (5)$$

It appears reasonable to assume that the cloud configuration in convectively active and overcast regions would tend to be of maximum overlap. In the region of less cloudiness, on the other hand, the cloud configuration would tend to be of minimum overlap. In the present program, we use the maximum overlap assumption whenever there is high cloud cover appearing in the grid box. Otherwise, a minimum overlap assumption is used.

2.2 Radiative Transfer Parameterization

The raditive transfer parameterization program used in this study follows that developed at the University of Utah. It is based on a broadband method and involves the transfer of thermal IR and solar radiation in both clear and cloudy regions. In a clear atmophere, the entire IR spectrum is divided into five bands: three for H_2O, one for CO_2, and one for O_3 absorption. The parameterizations of these broadband IR emissivities were developed by Liou & Ou (1981), and Ou & Liou (1983). The solar spectrum consists of 25 bands six for H_2O, one for CO_2 which overlaps the H_2O 2.7 band and 18 for O_3. Parameterization of the broadband solar absorptivities for these absorbers was documented in Liou *et al.*(1984).

In a cloudy atmosphere, low and middle clouds are treated as blackbodies in an IR radiative transfer calculation. The broadband IR emissivity, reflectivity, and transmissivity for high clouds as well as the broadband solar absorption, reflection, and transmission values for various cloud types are computed based on the prescribed vertical cloud liquid water content. Cloud radiative properties are calculated based on the parameterizations developed by Liou & Wittman (1979). Accuracy of all the aforementioned parameterizations was verified via more comprehensive and exact radiative transfer calculations described by Ou & Liou (1988).

The radiative heating rate at level Z is related to the divergence of the net fluxes and is given by

$$\Delta F(Z) = F^{\uparrow}(Z) - F^{\downarrow}(Z)$$

$$\frac{\partial T}{\partial t} = -\frac{1}{\rho C_p \Delta Z} \ \Delta F(Z) \qquad (6)$$

where ρ is the air density, C_p the specific heat at constant pressure, ΔZ is the model layer thickness and ΔF is the net radiative flux difference between the layer top and bottom. This equation applies to both IR and solar heating rate calculations with the downward solar flux and the upward IR flux defind as positive. For the transfer of solar radiation in a cloud layer, the net flux density decreases from the cloud top to the bottom because of cloud absorption and scattering. The absorded radiant energy leads to the heating of the cloud layer. For black clouds (low or middle clouds), the IR radiative flux is proportional to the fourth power of the absolute temperature of the cloud. Since the atmospheric temperature usually decreases with height, the downward IR flux emitted by the atmosphere above a black cloud top is much smaller than that emitted upward by the black cloud. As a result, the net flux near the cloud top is greater than zero and leads to strong IR cooling in the region. Similarly, there is IR heating near the cloud bottom. For a nonblack high cloud, the intracloud flux profile is determined by exponential interpolation between the fluxes at cloud top and base.

For partly cloudy conditions, the radiative heating/cooling rate at each model layer is obtained by linearly weighting the percentages of the total cloud cover η, and the clear portion, ($1-\eta$), in the form

$$[\frac{\partial T}{\partial t}]^{pc} = \eta[\frac{\partial T}{\partial t}]^c + (1 - \eta)[\frac{\partial T}{\partial t}]^{nc} \qquad (7)$$

where the superscripts P_c, c , and N_c represent partly cloudy, cloudy, and clear conditions, respectively. This equation applies to both IR and solar heating rate calculations. Detail descriptions of the present model for the parameterization of radiative flux exchanges in the three–deck cloudy atmosphere have been documented in Ou & Liou (1988).

3. RESULTS

3.1 Background of TAMEX IOP-2

The IOP–2 observation period started at 0600 UTC 16 May, 1987. The Mei–Yu front, accompanied by a weak squall line and its associated mesoscale convective systems over the Taiwan Strait, reached northern Taiwan in the early morning of 17 May. From surface analysis we see that a weak frontal system was hanging over the southern part of mainland China at 1200 UTC on the 16th. By 1800 UTC, the front was approaching the northern tip of the island and was oriented northeast–southwestward. At 0000 UTC 17 May, the surface front had passed through northern Taiwan. Relative vorticity at 850mb for 0000 UTC 16 May showed that the axis of maximum vorticity was close to the frontal position and intensified as time progressed. The potential temperature gradient along the front was relatively weak. The environmental flow prior to the passage of the Mei–Yu front was characterized by a strong southwesterly flow up to 500mb in advance of a short wave trough west of Taiwan. As the front moved over central Taiwan, it showed down and eventually stagnated over the Bashi Channel on the morning of 18 May. The system led to more than 50 mm of daily rainfall over northern and central Taiwan; it also caused about 60 mm daily rainfall over southern Taiwan. Additionally a record–breaking hourly rainfall of 89 mm and excessive daily rainfall of 275 mm were measured at Tongchitau (Lin & Lin , 1990), which is an island station in the Taiwan Straits. For a detailed evolution of synoptic scale patterns, the reader is referred to Chiao *et al.* (1988).

3.2 The Data

The atmospheric data from ECMWF/WMO analysis data sets on May 16–17, 1987, are used as input to the present cloud/radiation model. These data contain temperature and specific humidity on all 7 layers (i.e. 1000, 850, 700, 500, 300, 200 and 100mb) with a horizontal grid of 2.5 latitude/longitude. The diagnosed surface pressure is also included.
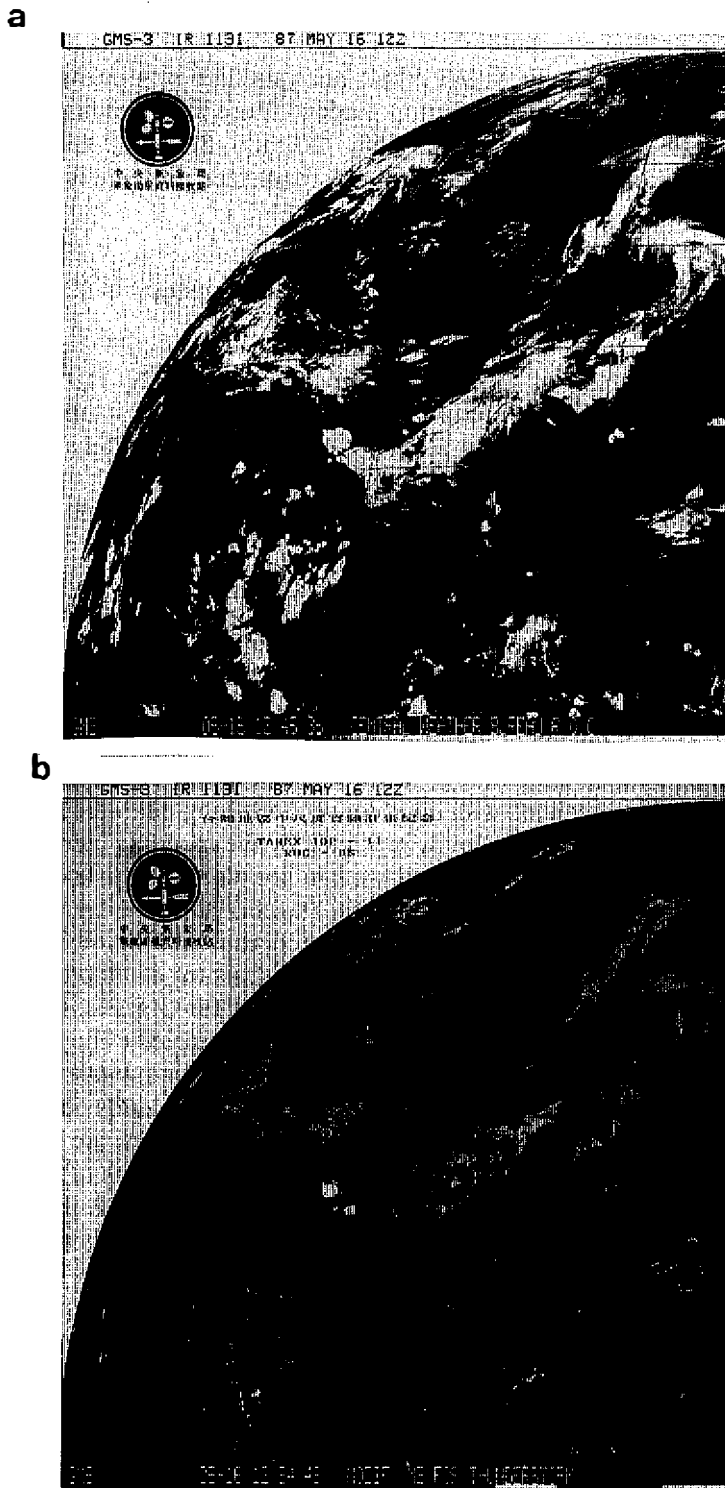
3.3 Cloud Cover

Figure 2a–b show the GMS–3 infrared and enhanced IR images at 1200 UTC 16 May, 1987. From those figures we can see:

(a) A pronounced bright zone of cloudiness extending from 20°N, 110°E northeastward to south of the Japanese islands; this corresponds to the Mei–Yu front on the surface weather map. The other bright band is located over northeasten China and is associated with a clod front.

(b) Deep convection surrounded by stratiform clouds is located in southern China, just north of the South China Sea.

(c) Areas of little cloudiness are scattered around Indo–China and the Tibetan plateau.

Utilizing the initial field of 1200 UTC, 16 May 1987, (which consists of temperature and specific humidity) the cloud fields are generated. Figure 3a–d show the geographical distribution of the high–, middle–,low–level and total cloud covers calculated by the cloud scheme, with corresponding gray values given in the lower right–hand corner. The darker the cloud picture, the larger the cloud cover is. Also in the figure the minimum cloud cover contour line is 20%. The distribution of high–level cloud (Figure 3a) shows discrete areas of cloudiness; the anvil cirrus associated with deep convection along the Mei–Yu and cold fronts is well–represented. The middle-level clouds predicted by the model (Figure 3b) appear very similiar to the IR image (Figure 2a); from it we can see clearly the Mei–Yu frontal cloud zone. The predicted low–level clouds (Figure 3c) appear to have captured the areas of stratus and stratocumulus in the region over the tropical oceans and the Mei–Yu frontal zone.

Verification of cloud distribution at different levels presented some problems. Although ground–based cloud cover observations have been recorded for decades, the cloud amount obtained by a ground observer, tends to be subjectively overestimated (Hughes, 1984) and is less reliable at night. For multilayer cloud conditions, the cloud amounts associated with the upper cloud layers are frequently underestimated due to the lower clouds obscuring the upper clouds. In contrast to surface–base observations, satellite observations are objective and the infrared sensors on board satellites can provide night–time observations of as good a quality as those taken in daytime. Satellite observations tend to underestimate the cloud amounts associated with the lower cloud layers, which are obscured by the higher cloud layers. In addition, there is substantial error arising from the failure to distinguish between snow/ice surfaces and cloud tops, especially in the polar regions. Nevertheless, satellite observations provide an even global scope of cloud cover with a resolution as high as 48 Km by 48 Km per pixel. This high resolution satellite observed cloud cover makes satellite observations superior to other cloud observations. Comparing the simulated cloud fields (Figure 3) with the infrared image (Figure 2) shows that the present scheme has been reasonably successful in reproducing the main features of cloud distribution at 1200 UTC 16 May.

Figures 4a–b show the GMS IR images at 0000 UTC 16 and 17 May 1987, respectively. From Figure 4a we can find several areas of bright cloud zones, among them, a mesoscale
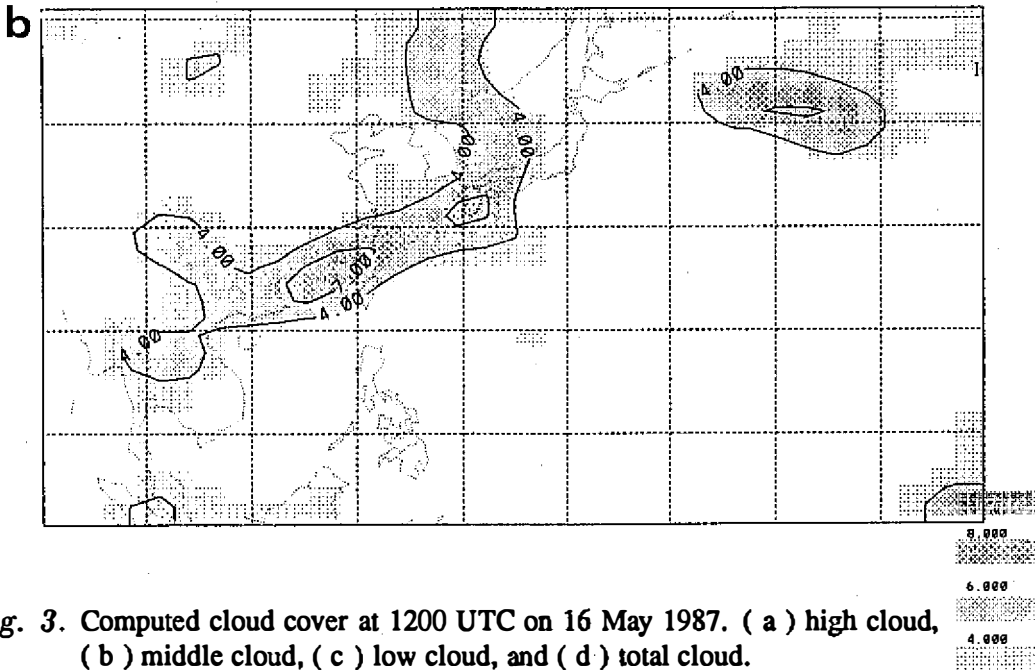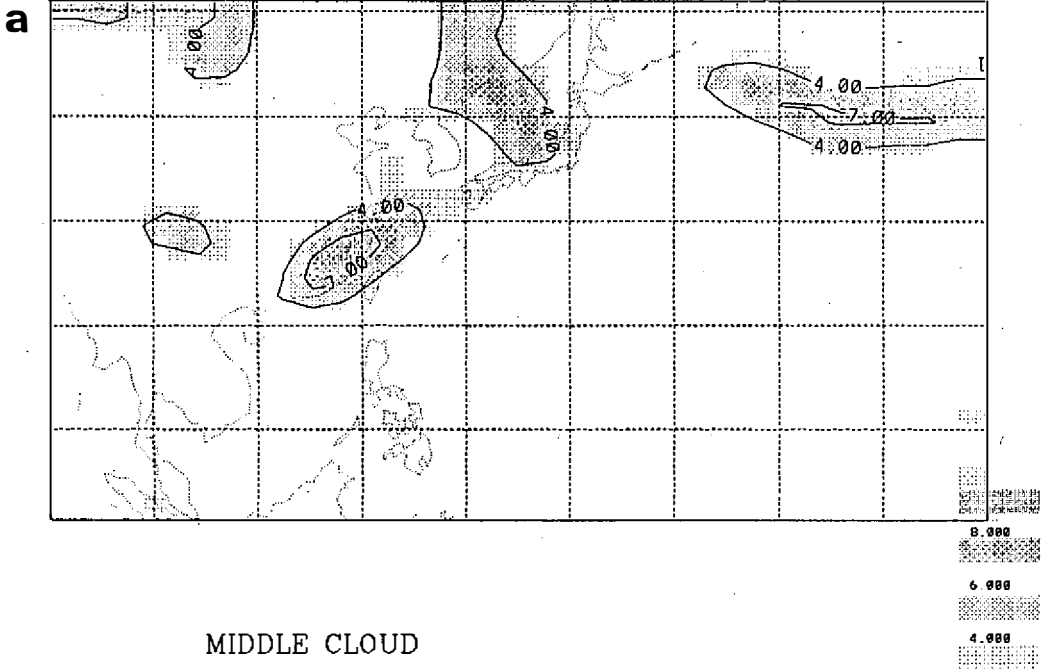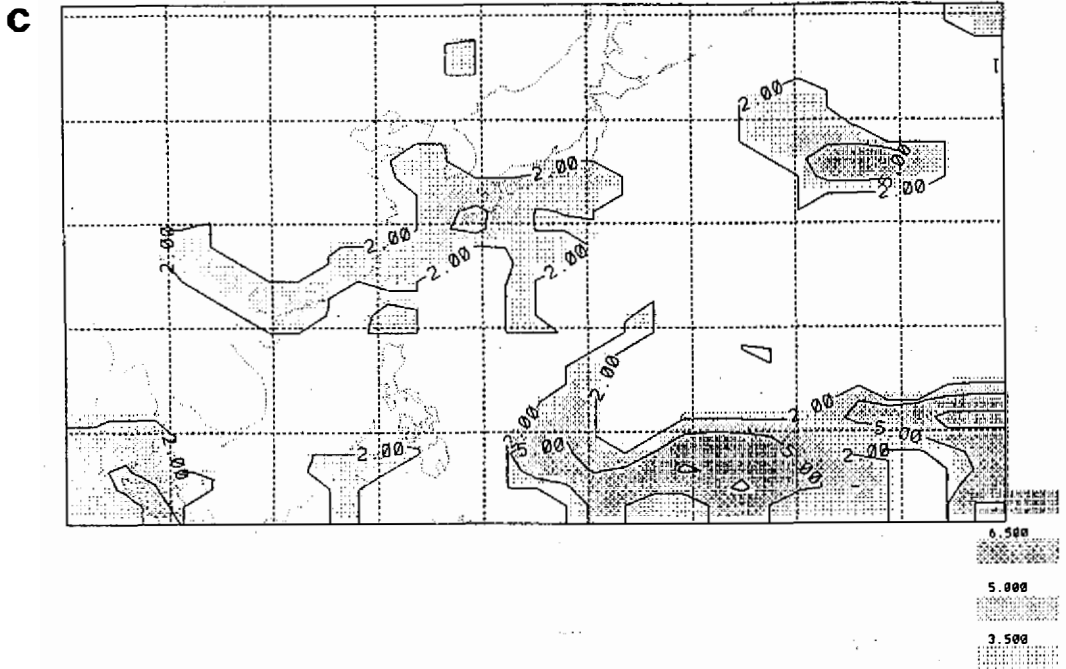
a

b

Fig. 2. Infrared images of GMS–3 for 1200 UTC on 16 May 1987. (a) IR, (b) enhanced.

HIGH CLOUD   87051612Z

a

MIDDLE CLOUD

b

Fig. 3. Computed cloud cover at 1200 UTC on 16 May 1987. (a) high cloud, (b) middle cloud, (c) low cloud, and (d) total cloud.
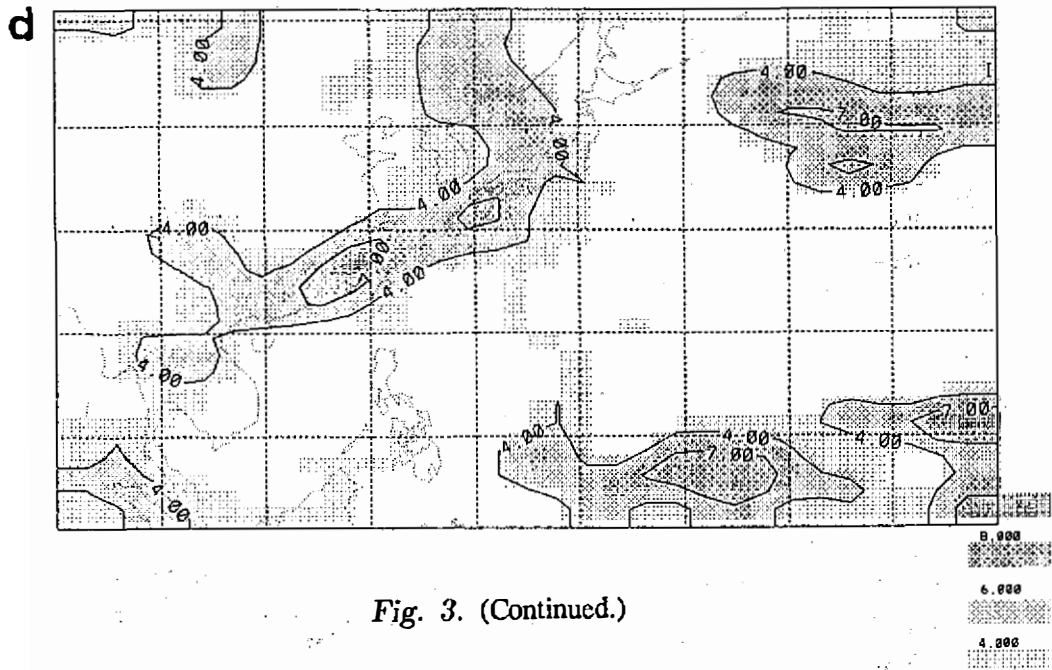
LOW CLOUD

c

TOTAL CLOUD

d

Fig. 3. (Continued.)

a

b

Fig. 4. Infrared images of GMS–3 at (a) 0000 UTC, 16 May and (b) 0000 UTC, 17 May 1987.

convective system (MCS), located on the western side of Taiwan, cloud be easily recognized. On Figure 4b we can see organized bright cloud bands extending along the surface of the Mei–Yu front from 15°N, 115°E northeastward to 40°N, 115°E. There were also several MCS embedded in this cloud band.

Figures 5a–b show simulated total cloud cover distributions by using the initial field of 0000 UTC, 16 & 17 May 1987. Comparing Figure 5a with Figure 4a, the MCS on the western side of Taiwan was simulated. The other bright cloud zones also reliably predicted. From Figure 5b we can see a pronounced cloud cover band oriented in a NE–SW direction with three clusters (cloud cover > 70%).

Generally speaking, the comparison between computed and satellite–observed IR cloud cover during the TAMEX IOP–2 period is quite encouraging.

3.4 Radiation Budget and Radiative Cooling Rate

Using the aforementioned data with the Ou & Liou (1988) radiation programs, the distributions of outgoing IR fluxes (OLR, unit: W/m^{-2}) at the model top and the net radiative heating rate (°C/day) at the high–level cloud top were generated and are illustrated in Figures 6a, 6c, 7a, 7c, and 8a, 8c, respectively. The satellite derived OLR distribution with a horizontal grid of 2.5 latitude/ longitude are shown in Figures 6b, 7b, and 8b.

In tropical latitudes where surface temperature contrasts are small in most areas, low OLR values corresponding to regions of high cloudiness are associated with deep convection. In higher latitudes, the interpretation is less clear, because low surface temperature also produce a low OLR reading. In this report contours which indicate an OLR of less then 220 Wm^{-2} are showen in Figures 6b, 7b, and 8b, in order to present the areas where there are clouds with relatively high cloud tops. Therefore, the Mei–Yu front corresponding to the low OLR area can be easily identified in those figures.

3.4.1 1200 UTC 16 May, 1987

From Figure 6b, it is seen that deep convection is concentrated in several regions during 1200 UTC 16 May, 1987. Among them, a low OLR zone extended from Japan southwestward to the southeast coast of the mainland and then it turns north and northwest along the southern peripheral of the Tibetan plateau. The others are located around 165°E, 41°N and the central tropical Pacific. Comparing Figure 6b with Figure 2, we can see that the low OLR areas coincide with regions of high cloudiness associated with deep convection. Figure 6a shows the simulated OLR distribution. It appears that the simulated OLR patterns are in agreement with the observations (Figure 6b). The Mei–Yu frontal band and a low OLR center around 165°E, 40°N are well represented. The major difference between the computed and observed OLR distribution occurs at 108°E, 18°N. This area needs more attention. From Figure 6b we can see there is a low OLR center with a minimum value of 125 Wm^{-2}. This suggests that deep convection is occurring. However, from Figure 2 we find that this area is cloudless. Our simulation also shows it is cloudless area. The reason for this discrepancy is not clear, however, it might be caused by thin cirrus. As mentioned by Liou (1986): " The identification of thin cirrus by using IR temperature techniques from satellite is extremely difficult, in view of the fact that they are far from blackbodies.". It is necessary to have a global cirrus cloud climatology including cloud cover, height and thickness. However, the determination of reliable cirrus cloud height and thickness information will require additional efforts. From Figure 6b and Figure 3 we find that the low OLR regions coincide with the high cloud areas,

TOTAL CLOUD   870516ØØZ   CLOUD

a
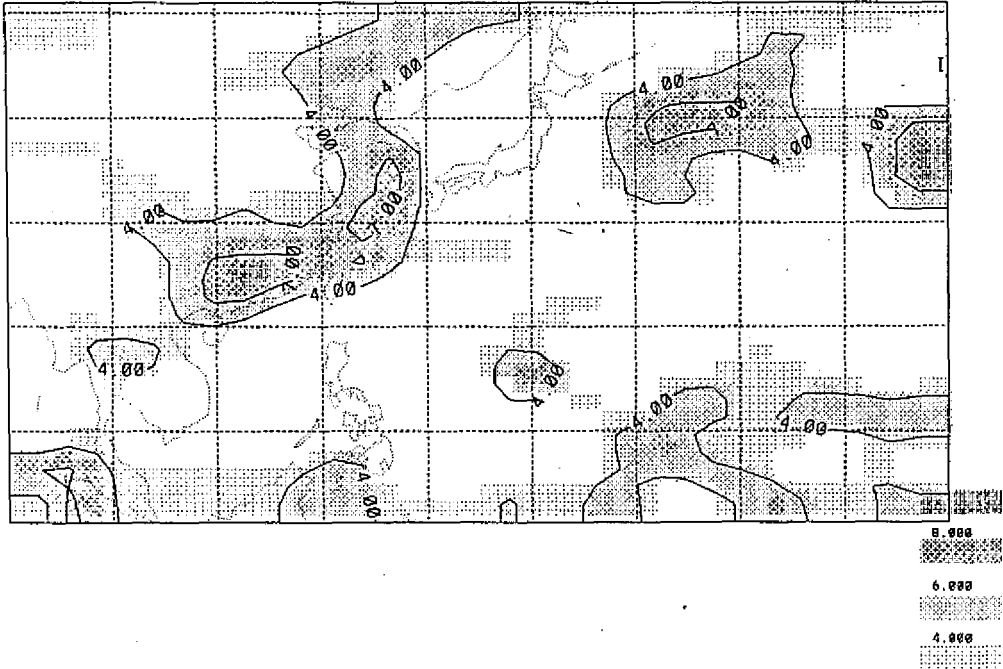
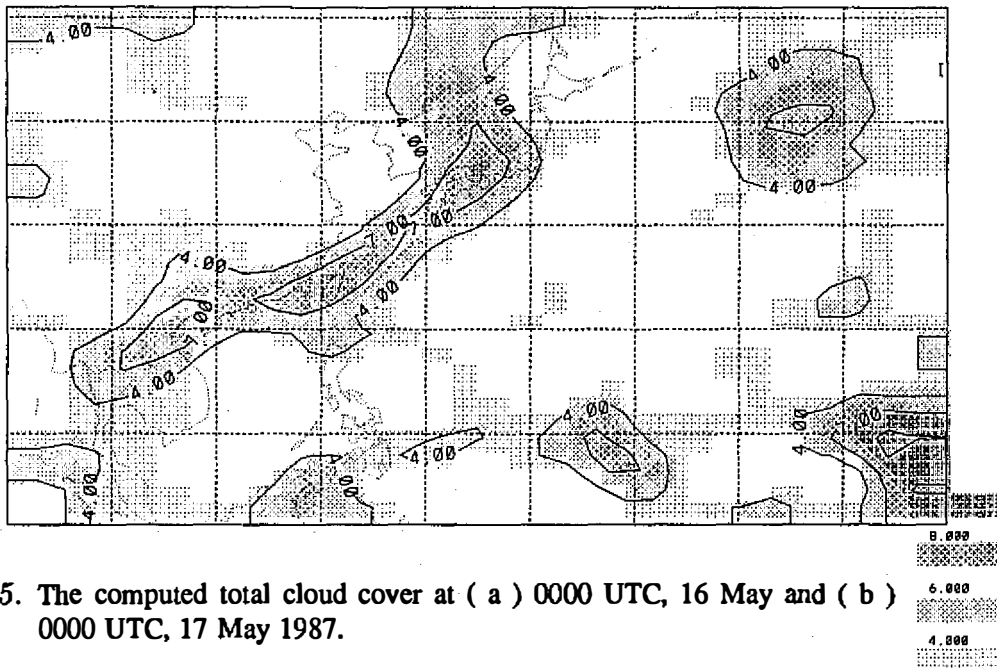TOTAL CLOUD   870517ØØZ   CLOUD

b

Fig. 5. The computed total cloud cover at (a) 0000 UTC, 16 May and (b) 0000 UTC, 17 May 1987.

87051612Z

Fig. 6. The computed and satellite–derived outgoing long wave radiation (OLR
) fluxes (Wm^{-2}) at the top of present model as well as the net radiative
heating (°C/day) at the high–level cloud top, at 1200 UTC, 16 May 1987.
(a) computed OLR, (b) satellite–derived OLR, and (c) net radiative
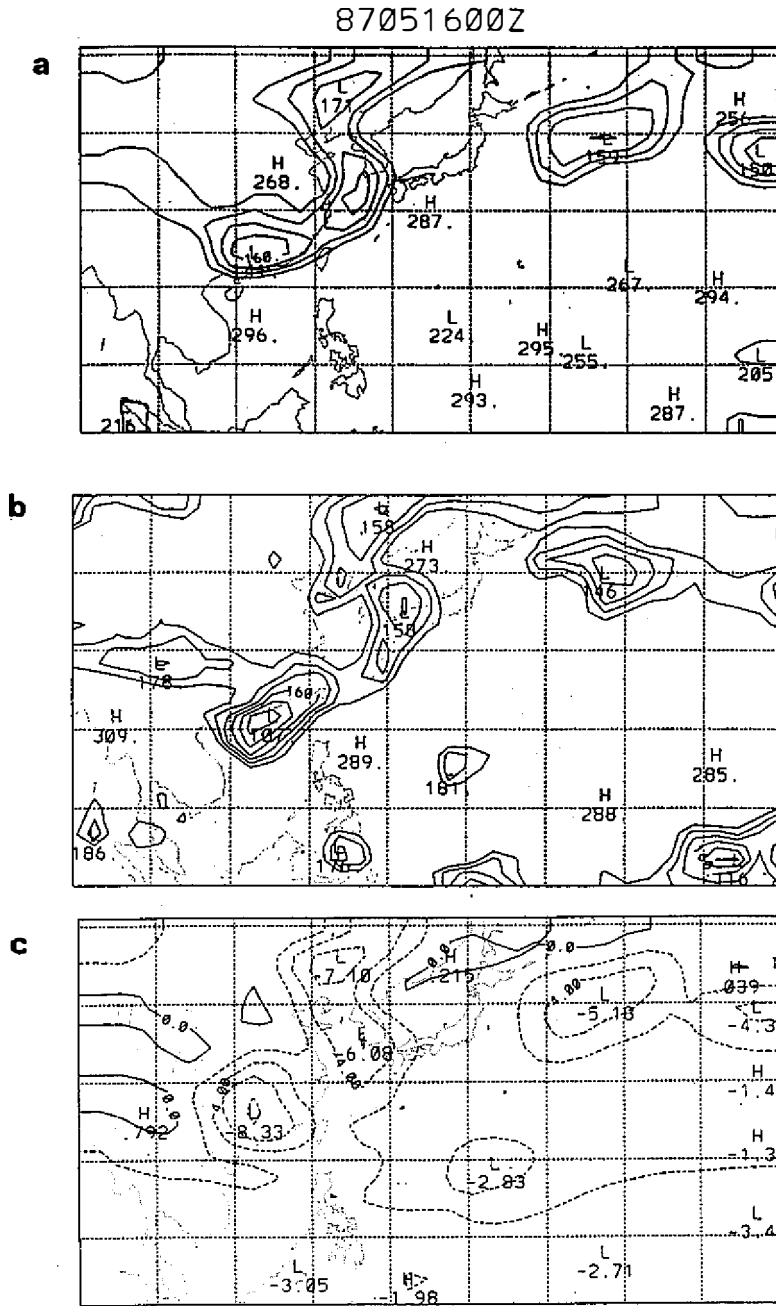heating.

870516002

Fig. 7. The computed and satellite–derived outgoing long wave radiation (OLR) fluxes (Wm^{-2}) at the top of present model as well as the net radiative heating (°C/day) at the high–level cloud top, at 0000 UTC, 16 May 1987. (a) computed OLR, (b) satellite–derived OLR, and (c) net radiative heating.
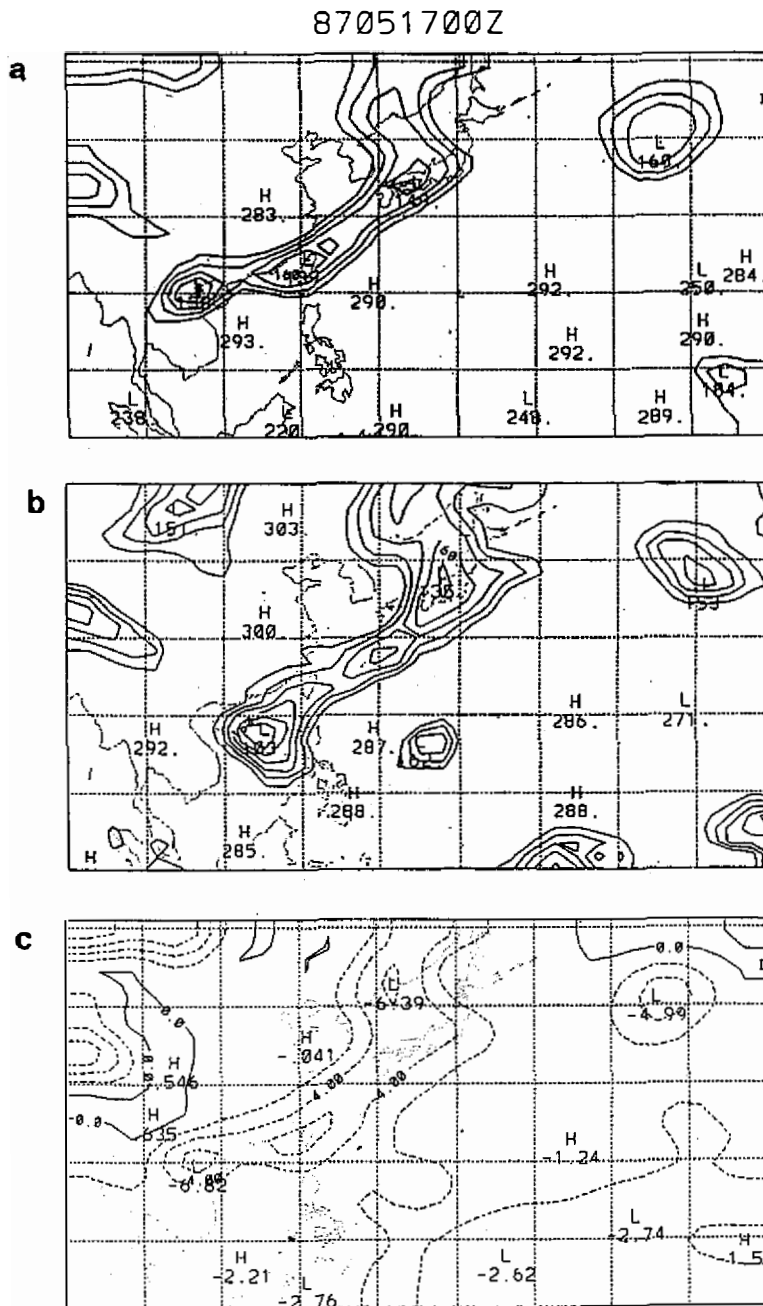
87051700Z

Fig. 8. The computed and satellite–derived outgoing long wave radiation (OLR) fluxes (Wm^{-2}) at the top of present model as well as the net radiative heating ($°C$/day) at the high–level cloud top, at 0000 UTC, 17 May 1987. (a) computed OLR, (b) satellite–derived OLR, and (c) net radiative heating.

as would be expected. Figure 6c shows the net radiative heating rate distribution at the top of the model's high–level cloud. Basically, the pattern of the net cooling rate is the same as that of the computed low OLR distribution and it is closely related to the high cloud cover contour (Figure 3a). From this figure, it is seen that there is a strong cooling band with a cooling rate of greater than 4°C/day along the Mei–Yu front. The maximum cooling rate on this cooling band is 12°C/day and it is located at 26°N, 117°E. In the meantime, the computed net radiative heating/cooling rate in the low level cloud base is very weak (figure not shown).

3.4.2 0000 UTC 16 May, 1987

At this period the front at 850 mb was oriented in a NE–SW direction extending from 33°N, 11°E to 23°N, 116°E. Deep convection can be seen in several regions (Figure 7b). Among them, one low OLR zone extended from Japan southwestward to the southeast coast of the mainland. We can also find three low OLR centers; one around the southeast edge of the Tibetan plateau and the other two around 157°E, 40°N, and 174°E, 3°N, respectively. The minimum value of the OLR is 107 Wm^{-2} and is located at 22° N, 115° E. Figure 7a shows the simulated OLR map. Comparison with Figure 7b shows a good simulation of many features such as the low OLR band, with the minimum over 157° E, 40° N. However, there has been disagreement, such as over the Tibetan plateau and over 174°E, 3°N. These differences can be identified as errors in the model's simulation of the high–level cloudiness. The cloudiness in this simulation in general is underestimated. Therefore, the OLR values are overestimated by the model. Figure 7c shows the net radiative heating rate at the top of high–level cloud. The maximum cooling rate is 8.3°C/day and it located around 24°N, 112°E, where the deep cumulus clouds over the front can be identified as in Figure 4a. Other larger cooling rate centers are at the NE edge of the front with a cooling rate of 6°C/day and at 157°E, 40°N with a cooling rate of 5.2°C/day. At the low–level cloud base the computed radiative heating rate is very small along the front.(figure not shown).

3.4.3 0000 UTC 17 May, 1987

During this time , the surface front had passed thrugh northern Taiwan, and the convective cloud clusters along the Mei-Yu front are more mature. From the observed OLR map (Figure 8b) we can see three low OLR centers along the 850mb Mei-Yu front. Those three low centers clustered together to form a low OLR band corresponding to the Mei–Yu front. There also are several low OLR centers around the tropical equator. Figure 8a shows a computed OLR distribution which is very similar to that in Figure 8b. The low OLR zone with three low centers on it can be easily seen. Figure 8c shows the computed net radiative heating distribution at the top of the high–level cloud. We find that along the Mei–Yu front the cooling rate is greater than 4°C/day with a maximun value of 6.8°C/day. It is also noticed that the cooling rate over the Taiwan area is greater than 6°C/day.

4. CONCLUSION

The role of clouds in atmospheric circulation appears to be paradoxically dual. On the one hand, organized cloud ensembles owe their origin to large–scale dynamical forcing, while on the other hand, they provide one of the most important mechanisms for vertical redistribuation of heat and moisture and momentum on the large scale. Clouds reflect incoming

solar radiation and thereby reduce the total solar energy available to the earth–atmosphere system. They also absord and emit terrestrial radiation, thereby reducing the net outgoing thermal radiation. The lifetime of all individual cases of Mei–Yu fronts over southern China range from 3 to 22 days (Chen, 1983) with a nearly continuous cloud band accompaning this front. It is the goal of this study to estimate the cloud's radiative effects on the Mei–Yu front.

The present radiative transfer model is based on a broadband method and involves the transfer of IR and solar radiation in clear and cloudy regions (Ou & Liou, 1988). To perform radiative transfer calculations and to compare with observed cloudiness, the model–predicted cloud covers are divided into low, middle and high clouds, which overlap each other in a maximum or minimum manner.

The result of the cloud scheme adopted in this paper to compute cloudiness during the TAMEX IOP–2 periods have shown a reasonable degree of success. From calculations we can find that the nearly continuous cloud band over the Mei–Yu front is dominated by middle–level cloud, and this cloud band is organized into several dense clouds which are strongly linked to high–level deep cumulus. The predicted total cloud pattern is very similar to the observed satellite cloud picture. However, cloudiness in general is underestimated by the model, especially for high–level cloud. The reason for this may be identified as the analysis data having come from the synoptic scale data.

The radiation model calculated radiative net flux as well as the heating/cooling rate based on the predicted cloud cover with a 12–layer structure. Observing the model–predicted cloud cover and OLR fields, as we would have expected, the OLR patterns are basically controlled by the predicted cloud cover. In the Mei–Yu frontal zone the computed OLR's value is less than $220 \ Wm^{-2}$ with several minimum centers embedded in it. Comparing the predicted OLR patterns with the satellite–derived OLR data, we find that the simulated patterns are in agreement with the observations. Nevertheless, the OLR fluxes over the Mei–Yu frontal zone and the tropical convection areas, are bigger than the observed ones. These differences are mainly caused by the underestimation of the high–level cloud's cloudiness.

The distribution of the computed radiative heating and cooling rate have very different vertical profiles. For solar radiation, maximum heating during the daytime (0000 UTC, 16 & 17, May) is about 5°C/day at the top of the middle–level cloud. For the IR radiation, the maximum cooling rates occurred in the high–level cloud top and they are greater than 10°C/day. For the net radiative heating rates, it is seen that the maximum heating for the three computed periods is less than 3.5°C/day. Nevertheless, the maximum net cooling rates are much greater than the heating rates and are all located at the same positions as for maximum IR cooling. For each individual period we will only emphasize the net cooling rate at the high–level cloud top. At 0000 UTC 16, the cooling rate around the Mei–Yu front is greater than 2°C/day, the maximum cooling is 8.3°C/day and located at 112°E, 24°N. Twelve hours later (1200 UTC 16), the cooling is more intense. Over the Mei–Yu front, the cooling rate in general is larger than 6°C/day and the maximum cooling changed to 12°C/day located at 118°E, 26°N. At the same time, we can find over the SE edge of the Tibetan Plateau, another cooling center with a cooling rate of 9.2°C/day. At 0000 UTC 17, the cooling rate over the Mei–Yu front is weaker and the cooling center SE of the Tibetan has disappeared. There were two cooling centers along the Mei–Yu front, both around 6°C/day. One is located at 19°N, 107°E and the other is over the Taiwan. It is noticed that the cooling rate over the Taiwan area is greater than 6°C/day for both the 1200 UTC 16 and 0000 UTC 17 periods.

From the above results we conclude that during the TAMEX IOP–2 period along the Mei–Yu front, the maximum net cooling rate is concentrated in the upper troposphere ($\geq$

6°C/day), while the minimum heating/cooling is on the lower level ($\cong$ 1 ～ 2°C/day). Because the cloud top cooling exceeds cloud base warming, there is a net radciative cooling along the front. Of particular importance in the distribution net radiative cooling is the co-existence of the area with largest cooling and areas of deep convection. There must be a direct interaction between convective heating and the radiative cooling.

Finally, it should be emphasized that our conclusions are highly dependent on accurate estimates of cloudiness. Although the present cloud parameterization scheme cloud be criticized for its lack of scientific basis, it has at least provided a reasonable prediction of cloudiness. However, the verification of these cloud distributions presented some problems. Experimental programs like ERBE FIRE and ICE are designed to understand the various processes of dynamics, thermodynamics, cloud microphysics and radiative transfer and the complex way these processes interact with each other. These process studies deal with phenomena on a wide range of scales varying from the microphysical scale up to the cloud scale and the mesoscale. With more effort both from the point of view of basic observations, and in the context of process study experiments we will hopefully improve the present cloud parameterization scheme.

REFERENCES

Chen, G. T. 1983: Observational aspects of the Mei–Yu phenomenon in subtropical China . *J. Meteor. Soc.* Japan, **61**, 306-312.

Chiao, F. L., L. S. Fang, and W. S. Kau, 1988: Taiwan Area Mesoscale experiment. Weather maps (Part I and Part II). Central Weather Bureau Report No. 233, Taipei, Taiwan.

Geleyn, J. F., 1981: Some diagnostics of the cloud/radiation interaction in ECMWF forecast model. Proceedings Workshop on Radiation and Cloud-Radiation Interaction in Numerical Modeling, ECMWF, Reading, England, 135-162.

Hughes, N. A., 1984: Global cloud climatologies. A historical review. *J. Clim. Appl. Meteor.*, **23**, 724-751.

Kato, K., 1985: On the abrupt change in the structure of the Baiu front over the China continent in late May of 1979. *J. Meteor. Soc. Japan*, **63**, 20-35.

Liou, K. N., and G. D. Wittman, 1979: Parameterization of the radiative properties of clouds. *J. Atmos. Sci.*, **36**, 1261-1273.

Liou, K. N., and S. C. Ou, 1981: Parameterization of infrared radiative transfer in cloudy atmospheres. *J. Atmos. Sci.*, **38**, 2707-2716.

Liou, K. N., and S. C. Ou, 1983: Theory of equilibrium temperatures in radiative–turbulent atmospheres. *J. Atmos. Sci.*, **40**, 214-229.

Liou, K. N., and Q. Zheng, 1984: A numerical experiment on the interactions of radiation, clouds and dynamic processes in a general circulation model. *J. Atmos. Sci.*, **41**, 1513-1535.

Liou, K. N., S. C. Ou., S. Kinne, and G. Koenig, 1984: Radiation parameterization programs for use in general circulation models. Report No. AGFL–TR–84–0217, Air Force Geophysics Laboratory, Hanscom AFB, MA, 53 pp.

Liou, K. N. 1986: Influence of cirrus clouds on weather and climate processes: A global prespective. *Mon. Wea. Rev.,* 114, 1167-1198.

Lin, M. S., and S. M. Lin, 1990: The comparison of enviromental conditions among selected mesoscale convective systems during TAMEX period, Preprints, Workshop on TAMEX Scientific Results, 24-26 September 1990, Boulder, Colorado, 103-108.

Ninomiya, K. and T. Murakami, 1987: The early summer rainy season (Baiu) over Japan, Monsoon Meteorology, edited by C. P. Chang, and T. N. Krishnamurti, Oxford, Clarendon Press, 93-127.

Ou, S. C. and K. N. Liou, 1988: Development of radiation and cloud parameterization programs for AFGL global models. Report No. AFGL–TR–88-0018, Air Force Geophysics Laboratory, Hanscom AFB, MA, 88 pp.

Slingo, J. M., 1987: The development and verification of a cloud prediction scheme for the ECMWF model. *Quart. J. Roy. Meteor. Soc.,* 113, 899-927.

Slingo, J. and B. Ritter, 1984: Cloud prediction in the ECMWF model. ECMWF Technical Report No. 46, Reading, England, 49 pp.

Sunqvist, H., 1978: A parameterization scheme for non–convective condensation including prediction of cloud water content. *Quart. J. Roy. Meteor. Soc.,* 104, 677-690.